JOURNAL OF SPACECRAFT AND ROCKETS
Vol. 33, No. 6, November–December 1996

Coning Instability of Spacecraft During Periods of Thrust

R. X. Meyer*
University of California, Los Angeles, Los Angeles, California 90095

An instability that has been observed in the flight of a number of spin-stabilized spacecraft is analyzed. These vehicles, all of which had solid-propellant motors, exhibited a pronounced coning during the motor burn. The analysis is based on a hydrodynamic model of liquid slag trapped in the motor and is closely related to the classic shallow fluid or tidal theory. Explicit, analytical results are derived for the case of small ratios of slag to vehicle mass and are illustrated with a numerical example that is typical of the vehicles for which the instability has been observed. Calculated are the growth rate of the instability and the theoretical gain needed for stabilizing the vehicle by a simplified control scheme.

Nomenclature

A_0 = cross-sectional area of fluid pool at reference condition, m^2
$\boldsymbol{a}$ = acceleration of vehicle center of mass, m/s^2
b_0 = width of free surface at reference condition, m
c_0 = zero-order wave speed relative to vehicle [Eq. (12)], m/s
$\boldsymbol{f}$ = inertial force per unit mass, m/s^2
h_0 = fluid height at reference condition [Eq. (9)], m
I_t, I_z = transverse and axial moments of inertia, m^2 kg
j_i = coefficients [Eq. (31)], nondimensional
l_i = polynomial coefficients [Eq. (36)], nondimensional
M = moment about center of mass, m N
$\dot{m}$ = rocket motor gas flow rate, kg/s
m_{fl} = fluid mass, kg
m_{vh} = vehicle mass, kg
N = nutation control gain, nondimensional
p = fluid pressure, N/m^2
q = wave height, m
R, ϕ, z = cylindrical, vehicle fixed coordinates; Fig. 2
R_c = mean radius of curvature of bounding surface (Fig. 3), m
R_f = mean radius of curvature of free surface, m
R_t = transverse gyroradius of vehicle, m
$\boldsymbol{r}$ = position vector, m
s = complex frequency [Eq. (25)], nondimensional
$\boldsymbol{T}$ = thrust, N
$\boldsymbol{u}$ = fluid velocity relative to vehicle, m/s
V, Q, R, A, Ω = complex amplitudes [Eq. (25)], nondimensional
v_1, w_1 = circumferential and meridional components of first-order perturbation velocity, m/s
x, y, z = Cartesian, vehicle fixed coordinates (Fig. 2), m
β_0 = angle relative to vehicle axis of zero-order inertial force [Fig. 2, Eq. (4)], rad
μ = mass ratio $m_{\mathrm{fl}}/m_{\mathrm{vh}}$, nondimensional
ν = lag angle of nutation control (Fig. 4), rad
ρ = fluid density, kg/m^3
σ = inertia ratio I_z/I_t, nondimensional
ϕ, η, ζ = vehicle fixed, toroidal coordinates; Figs. 2 and 3
ω = vehicle angular velocity, s^{-1}

Subscripts

j = jet damping
n = nutation control
p = fluid pressure
r, i = real, imaginary parts
t = transverse
0 = zero-order terms (referring to rotation about axis of symmetry)
1 = first-order perturbation terms

Received Dec. 4, 1995; revision received July 15, 1996; accepted for publication Aug. 13, 1996.

*Adjunct Professor, Department of Mechanical and Aerospace Engineering. Fellow AIAA.

Introduction

A NUMBER of spin-stabilized upper-stage space vehicles have exhibited a pronounced instability during the thrusting phase. The instability manifests itself primarily in an increase of the nutation angle, and is therefore referred to as nutational or coning instability. In all cases, these vehicles had solid-propellant motors with re-entrant nozzles. Although stable before and during roughly the first half of the rocket burn, the vehicles then started to precess with a nutation angle that was steadily increasing to the end of the burn. No further growth of the nutation angle was observed after thrust termination, except a very slow growth—of no particular concern—that can be explained by energy dissipation in the spacecraft. In some cases, the final nutation angle at thrust termination exceeded 15 deg.

The coning instability shows remarkably systematic properties. One of these is seen from Fig. 1, where for several different space vehicles the destabilizing moment about the vehicle's center of mass, as inferred from the observed rate-gyro and the vehicle's inertial data, is plotted against the instantaneous transverse component of the angular velocity.[1,2] The data roughly fall on a straight line through the origin, although different vehicles with different mass properties, somewhat different rates of spin, and different times after start of the instability are included. When translated by rigid-body mechanics, the data for this group of vehicles therefore indicate a near constant, exponential rate of growth. Although the final nutation angle reached at the end of the burn differs from case to case, the difference can be explained by small differences (less than 10% of the total burn duration) in the time of the onset of the instability.

Another important observation, derived from the rate gyros, was that the disturbing torque, whatever its origin, was synchronous with the precession of the vehicle (therefore not with the spin).

The data in Fig. 1 apply to earlier versions of upper-stage vehicles, before specially designed control systems were introduced. More recent vehicles use hydrazine or bipropellant control jets, which are pulsed in phase with the vehicle's precession whenever the nutation angle exceeds a prescribed threshold. These control systems proved to be quite successful in preventing the coning instability. However, because the cause of the instability remained uncertain, the control had to be greatly overdesigned. A basic understanding of the instability therefore is needed for estimating the required magnitude of the control authority in the design of new vehicles.

Various Explanations

At least six different explanations have been advanced at various times to explain the coning instability. The two most prominent

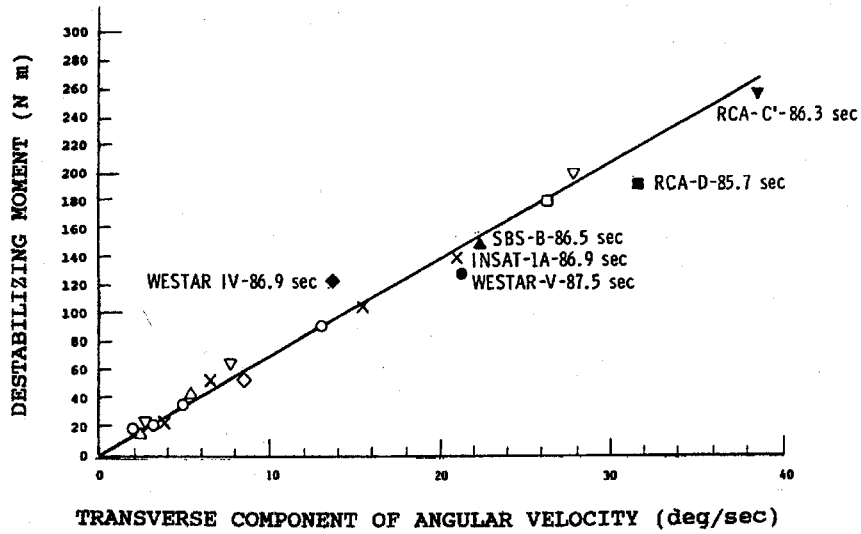

Fig. 1 Destabilizing moment inferred from flight gyro data (jet damping has been subtracted from the measurements).

among them and studied in considerable detail were 1) one based on the gasdynamics of the combustion gas and 2) one based on the motion of liquid slag trapped in motors with recessed (re-entrant) nozzles.

The gasdynamic hypothesis[1–4] postulates a convective instability of the gas in the rocket motor. It has been possible to show that in a precessing vehicle with nonzero nutation angle, a differential pressure of the gas on the motor case and nozzle will develop, resulting in a disturbance torque on the vehicle. For small nutation angles, this pressure difference is proportional to the excursion and has the proper phasing to drive the vehicle toward a higher nutation angle. The fact that the instability appears only relatively late in the motor burn has been explained in this hypothesis by the change in geometry as the propellant surface recesses.

These early studies, however, did not, or did only insufficiently, take into account the effect of the gas on the rocket motor nozzle. The gas enters it at an angle of attack proportional to the instantaneous nutation angle of the vehicle. But because of the rapid acceleration in the nozzle, the gas is largely redirected and exits the nozzle at an average angle to the motor axis that is greatly reduced. (Rocket nozzles with an entrance flow with angle of attack were studied as early as 1972 by Walters.[5] The most thorough work on such nozzle flows, both theoretical and experimental, has been carried out by Pirumov and Roslyakov.[6]) It then follows from conservation of angular momentum that the torque exerted by the gas on the motor case is largely, although not completely, canceled by an opposite torque exerted by the gas on the nozzle. This near cancellation also has been shown experimentally in a cold-flow experiment[7] and, more recently, by a detailed numerical study[8] of the gas flow in a precessing vehicle, taking into account the combined geometry of the motor chamber and of the nozzle. All of these more recent studies have indicated that, because of this compensation, the gasdynamic effect can be only a minor contributor to the observed instability.

Several investigators[9–11] have since proposed an explanation that invokes the presence, in the recess formed by re-entrant nozzles, of liquid slag (Al_2O_3 and Al) derived from aluminum-containing propellants. The mass of the slag, as a function of time, is an important parameter in the stability analysis, but is rather uncertain. The slag mass at the end of the burn can be measured for a given type of motor as part of ground testing. Usually, this type of motor is tested spinning, often in a horizontal position. However, because the axial acceleration of the flight vehicle is absent, the true slag mass can be inferred only by extrapolation from these tests, or by theoretical considerations.

In another study[12] a two-component gas/slag droplet model is presented that assumes that the trajectories of the larger droplets differ enough from the gas streamlines so as to become trapped in the recess formed by the nozzle and the motor case (or residual propellant). When this model is applied, the slag mass that is accumulated in the liquid pool is calculated at different times after startup. According to this model, the in-flight, final slag mass turns out to be considerably larger than the mass measured in ground tests. The difference is ascribed to the increased trapping caused by the acceleration of the flight vehicle.

A different model,[13] with the same objective, assumes that because of the very high level of turbulence of the gas in the motor, all particles that have entered the gas stream are swept out of the motor. The only slag trapped in the motor then is liquid slag flowing along the propellant surface, propelled by the spin-induced centrifugal force and, in-flight, by the vehicle's acceleration. This latter model results in in-flight slag masses that are not very different from those observed in ground tests.

The assumption that the sloshing of liquid slag is the cause of the observed instability is also made in this paper. The question of how much slag is really present in an accelerating vehicle can be related to the observed nutation instablity of these vehicles. A qualitative comparison of the slag masses inferred from the observed flight instability with those deduced from ground measurements is discussed in the Conclusions.

Physical Model

In this model, the instability is explained by the mutual interaction between the sloshing slag pool present in the rear part of the motor and the spinning and precessing vehicle. The onset of the instability relatively late into the motor burn is explained by the gradual buildup of the trapped slag as the burn progresses.

Several models have been proposed to describe the sloshing of the slag fluid and its interaction with the vehicle. The best-known analysis is the one by Mingori and Yam.[14,15] Here the slag is represented by a single point mass that can move in a plane perpendicular to the vehicle's symmetry axis and is acted upon by a restoring force proportional to the distance from the axis. No hydrodynamic analysis is made, but the model is important because of the basic insight it has provided.

In the present paper, a more complete description is made that takes into account, albeit approximately, the hydrodynamics of the slag trapped in the motor. Two modes of motion of the fluid are considered: First, gravity-type waves on the slag/gas free-surface, occurring as a consequence of the precession of the vehicle. These waves propagate around the annular configuration of the slag in the nozzle/motor case recess (Fig. 2), and second, wave motion at a right angle to the former, which corresponds to the fluid sloshing in the meridional direction along the solid boundary provided by either the motor case or the residual propellant.

The inclusion of both modes and of their interaction with the spacecraft dynamics has not been considered before. The analysis of the first type of mode follows the classic theory of tides.[16] The second type is a simple harmonic oscillator with a forcing term. The hydrodynamic description then is combined with the dynamics of the vehicle as described by Euler's rigid-body equations for spinning, inertially symmetric vehicles. The analysis leads to a characteristic fifth-degree polynomial. Explicit numerical solutions are obtained

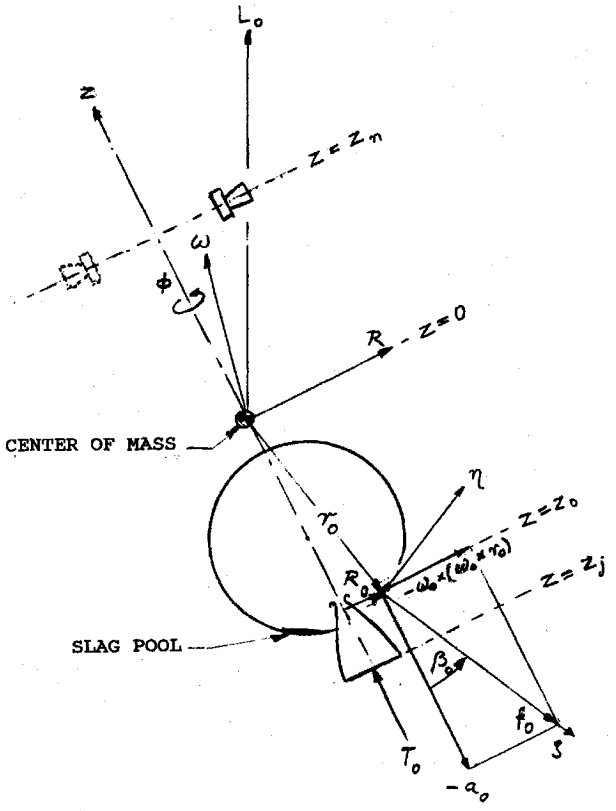

Fig. 2 Schematic of solid-propellant motor and spacecraft.

for the case, important in practice, in which the ratio of slag to vehicle mass is small. Also calculated is the minimum control authority of an idealized control system designed to avoid the instability.

Basic Assumptions

As is schematically indicated in Figs. 2 and 3, a spin-stabilized spacecraft is considered, propelled by the thrust of a solid-propellant rocket motor. The thrust is assumed to have constant magnitude, at least for a time interval long compared with the vehicle's precession period. The thrust line passes through the center of mass of the vehicle. (Here, and in what follows, the term "vehicle" will refer to the spacecraft proper, without the slag pool, which is accounted for separately.)

The viscosity of the slag at the temperature of the motor is low, and is neglected when considering the wave motion. However, because the time between spin-up of the vehicle and start of the burn is long, typically at least several minutes, even a small viscosity will be sufficient to spin up the slag so that it rotates with the vehicle.

Once the motor burn has started, the fluid, as a consequence of the thrust and of the spin, assumes the configuration of a fluid ring (Fig. 3). In practice, the slag volume is sufficiently small so that the ring's cross-sectional dimensions are small compared to the characteristic dimensions of the rocket motor. Therefore, the motion of the fluid is described by the motion of a one-dimensional fluid ring located at the centroid of the actual fluid, hence by just two independent variables: time and a single spacial (azimuthal) variable. The amount of fluid contained in any segment of the ring will vary because of the presence of the azimuthal waves. Also, the ring will distort from its equilibrium position in the plane perpendicular to the nominal spin axis. When disturbed, its parts move along the bounding surface, resulting in a meander-like configuration of the ring.

In rocket motors with re-entrant nozzles, more than one equilibrium configuration can occur, depending on the rate of spin and of the acceleration of the vehicle. They are schematically illustrated in Figs. 3b and 3c. For a sufficiently large rate of spin and low thrust, the fluid ring is high enough in the motor case to be unaffected by the nozzle geometry (Fig. 3b). In this case, the cross-sectional area A_0 of the fluid ring, at the reference condition (i.e., pure spin about the symmetry axis, with zero nutation angle), can be calculated readily as a function of the slag mass. The method is indicated in the

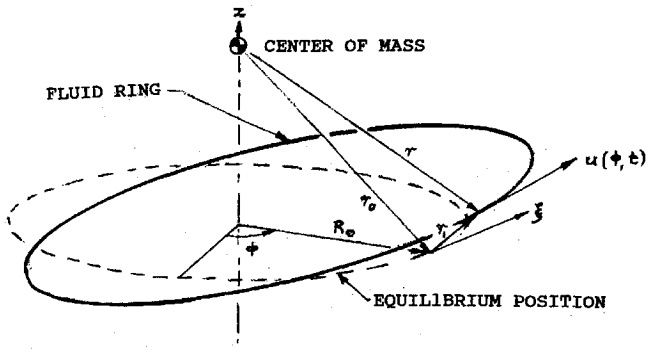

a) In reference position and in displaced position

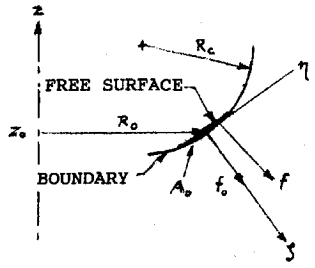

b) Cross section with circular arc boundary

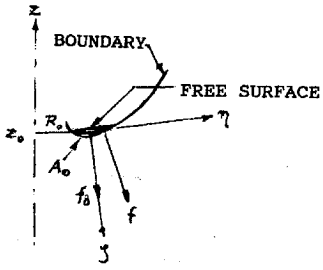

c) Cross section with general boundary (motor case and nozzle)

Fig. 3 Fluid ring.

Appendix. For lower rates of spin and higher vehicle acceleration, the fluid ring also may be partially bounded by the nozzle structure (Fig. 3c). In this case, the geometry is usually sufficiently complicated that a numerical integration of the fluid-ring cross section will be required.

As is commonly the case with spin-stabilized spacecraft, the vehicle is assumed to be inertially symmetric, i.e., to have equal transverse moments of inertia.

Inertial Forces

We introduce vehicle-fixed, cylindrical coordinates (R, ϕ, z) with the origin at the vehicle's instantaneous center of mass. (The time rates of change of mass and center-of-mass location are slow when compared to the precession period, and can therefore be considered as quasistationary.) Let $\omega(t)$ be the vehicle's angular velocity and $r(\phi, t)$ be the position vector extended from the vehicle center of mass to a point on the fluid ring. Also, let $u(\phi, t)$ be the fluid velocity relative to the vehicle and $a(t)$ be the acceleration of the vehicle's center of mass. The resultant f of all inertial forces in the vehicle-fixed reference frame that arise as a consequence of the vehicle motion, when divided by the slag mass, then takes the form

$$f = -a - \omega \times (\omega \times r) - \frac{\partial \omega}{\partial t} \times r - 2\omega \times u \qquad (1)$$

The subscript 0 henceforth designates the reference condition (i.e., the condition for which the vehicle is spinning with constant angular velocity about its axis of symmetry), and the subscript 1 designates the perturbation terms. Thus, $r_1(\phi, t)$ is the displacement in the $\phi =$ const plane of the fluid ring, characterizing therefore the meandering of the ring. Second-order terms are neglected. We let

$$r = r_0(\phi) + r_1(\phi, t), \qquad a = a_0 + a_1(t)$$

$$\omega = \omega_0 + \omega_1(t), \qquad u = u_1(\phi, t)$$

$$f = f_0(\phi) + f_1(\phi, t)$$

The zero-order acceleration of the vehicle center of mass and the thrust are related by

$$a_0 = T_0/m_{vh} \qquad (2)$$

and are assumed to be constant. If the perturbation terms are included, the trajectory of the vehicle's center of mass will be a spiral of increasing pitch.

From Eq. (1), omitting second-order terms,

$$f_0 = -a_0 - \omega_0 \times (\omega_0 \times r_0) \tag{3a}$$

$$f_1 = -a_1 - \omega_0 \times (\omega_0 \times r_1) - \omega_0 \times (\omega_1 \times r_0) - \omega_1 \times (\omega_0 \times r_0) - \frac{\partial \omega_1}{\partial t} \times r_0 - 2\omega_0 \times u_1 \tag{3b}$$

It also is convenient to introduce vehicle-fixed, toroidal coordinates (ϕ, η, ζ), with the center placed on a point of the fluid ring when in its reference position. The ζ axis is collinear with f_0, and the η axis is normal to it (Fig. 2). The angle between f_0 and the thrust axis (the z axis) is designated by β_0 and the radius of the fluid ring in the reference condition by R_0. Therefore,

$$\tan \beta_0 = \frac{\omega_0^2 R_0}{a_0}, \qquad \sin \beta_0 = \frac{\omega_0^2 R_0}{f_0} \tag{4}$$

The oscillation of the fluid ring takes place about a reference (or mean) position given by the coordinates R_0 and z_0. The resultant of $-a_0$ and $\omega_0^2 R_0$ must be perpendicular to the solid boundary and must be such as to ensure the static equilibrium of the fluid ring in its postulated reference position. The condition for static equilibrium is the inequality (5). It can be obtained by considering a virtual displacement by an arc length $d\eta$ of any element of the ring along the boundary. The resulting change in the angle β_0 is $d\beta_0 = d\eta / R_c$, where R_c is the local radius of curvature of the boundary. Also, $dR_0 = d\eta \cos \beta_0$. For neutral static stability, the resultant of $-a_0$ and $\omega_0^2 R_0$ must remain perpendicular to the boundary after the virtual displacement; hence

$$\tan(\beta_0 + d\beta_0) = \tan \beta_0 + d\beta_0 (1 + \tan^2 \beta_0) = \frac{\omega_0^2 (R_0 + dR_0)}{a_0}$$

to order $d\beta_0$. From this and Eq. (4) follows

$$\frac{R_c}{R_0} = (\cos^2 \beta_0 \sin \beta_0)^{-1}$$

For positive stability of the mean position of the fluid ring, R_c must be smaller, hence the inequality

$$\frac{R_c}{R_0} < \frac{1}{\cos^2 \beta_0 \sin \beta_0} \tag{5}$$

Let $P_1(t)$ be the perturbation force exerted by the fluid pressure on the vehicle. It is shown easily that, by symmetry, P_{1z}, and therefore also a_{1z}, vanish. Also, because the fluid's viscosity is neglected, the z-component of the moment of P_1 about the center of mass of the vehicle vanishes, with the consequence, which follows immediately, for instance, from Euler's rigid-body equation, that ω_{1z} vanishes. To summarize,

$$u_{1\zeta} = r_{1\phi} = r_{1\zeta} = a_{1z} = \omega_{1z} = 0 \tag{6}$$

to first-order accuracy. In what follows, we write, for short, v_1 for $u_{1\phi}$, w_1 for $u_{1\eta}$, and r_1 for $r_{1\eta}$.

It follows from Eq. (3b) that the components of the sum of the first-order inertial forces, per unit mass, acting on the fluid are

$$f_{1\phi} = d_{1x} \sin \phi - d_{1y} \cos \phi - 2\omega_0 w_1 \cos \beta_0$$

$$f_{1\eta} = \left(\omega_0^2 \cos \beta_0 r_1 + 2\omega_0 v_1 - d_{1x} \cos \phi - d_{1y} \sin \phi\right) \cos \beta_0 - (e_{1x} \cos \phi + e_{1y} \sin \phi) \sin \beta_0 \tag{7}$$

$$f_{1\zeta} = \left(\omega_0^2 \cos \beta_0 r_1 + 2\omega_0 v_1 - d_{1x} \cos \phi - d_{1y} \sin \phi\right) \sin \beta_0 + (e_{1x} \cos \phi + e_{1y} \sin \phi) \cos \beta_0$$

where

$$d_{1x} = a_{1x} + z_0 \left(\omega_0 \omega_{1x} + \frac{\partial \omega_{1y}}{\partial t}\right)$$

$$d_{1y} = a_{1y} + z_0 \left(\omega_0 \omega_{1y} - \frac{\partial \omega_{1x}}{\partial t}\right) \tag{8}$$

$$e_{1x} = R_0 \left(\omega_0 \omega_{1x} - \frac{\partial \omega_{1y}}{\partial t}\right) \qquad e_{1y} = R_0 \left(\omega_0 \omega_{1y} + \frac{\partial \omega_{1x}}{\partial t}\right)$$

Hydrodynamic Equations

The motion of the fluid in vehicle-fixed coordinates is described by the linear superposition of two modes: a surface wave with wave height $q_1(\phi, t)$, and a lateral displacement wave characterized by the meridional displacement $r_1(\phi, t)$ of the fluid along the solid boundary.

For the stability investigation, it is sufficient to include as the only perturbations those with wavelength $2\pi R_0$. For the higher harmonics, because of symmetry, the fluid pressure that acts on the boundary does not cause a net force or moment on the vehicle.

Surface Wave

Because the fluid volume is small compared to the motor volume, the fluid depth is small compared to the pertinent wavelength. This is just the condition for the shallow-water or tidal theory to be valid.[16,17] In the present instance, this theory needs to be augmented by the inertial forces produced by the vehicle's precession and nutation, as calculated in Eq. (7). The wave height is assumed to be small compared with the fluid depth, resulting in relations that will be linear.

Let

$$h_0 = A_0 / b_0 \tag{9}$$

To determine h_0 from the fluid volume generally requires an integration of the area between the boundary and the equilibrium free surface. A simpler method, appropriate when the boundary in the meridional plane is a circular arc (Fig. 3b), is indicated in the Appendix.

Consideration of the fluid volume bounded by the meridional planes ϕ and $\phi + d\phi$ constant results in the continuity equation for the fluid[16]:

$$\frac{\partial v_1}{\partial \phi} + \frac{R_0}{h_0} \frac{\partial q_1}{\partial t} = 0 \tag{10}$$

In deriving this equation, note that, as shown in tidal theory, the velocity is independent of the depth below the free surface.

Another result of tidal theory is that the pressure at a given location and depth is simply the pressure increment resulting from the height of the wave at that time and location, added to the equilibrium pressure. Therefore, if $H_0 = H_0(\eta, \zeta)$ designates the (positive) distance below the equilibrium free surface, the pressure $p = p(\phi, \eta, \zeta, t)$, after subtracting the ambient (constant) gas pressure in the motor, is

$$p = p_0 + p_1 = \rho(H_0 + q_1) f_\zeta = \rho(H_0 f_0 + H_0 f_{1\zeta} + f_0 q_1)$$

Differentiating with respect to ϕ and combining the result with Euler's equation for inviscous, incompressible fluids, it follows that

$$\frac{\partial v_1}{\partial t} = -\frac{1}{\rho R_0} \frac{\partial p_1}{\partial \phi} + f_{1\phi}$$

where second-order terms again have been neglected. Hence

$$\frac{\partial v_1}{\partial t} = -\frac{f_0}{R_0} \frac{\partial q_1}{\partial \phi} + f_{1\phi}$$

where, consistent with the prior assumptions, the term

$$-\frac{H_0}{R_0} \frac{\partial f_{1\zeta}}{\partial \phi}$$

has been neglected in comparison with $f_{1\phi}$.

By differentiating this last equation with respect to ϕ and Eq. (10) with respect to t, v_1 is eliminated, resulting in a wave equation with a forcing term

$$\frac{\partial^2 q_1}{\partial t^2} - \frac{c_0^2}{R_0^2} \frac{\partial^2 q_1}{\partial \phi^2} + \frac{h_0}{R_0} \frac{\partial f_{1\phi}}{\partial \phi} = 0 \tag{11}$$

where

$$c_0 = \sqrt{f_0 h_0} \tag{12}$$

is the phase velocity of the wave that propagates, in either direction, along the fluid ring.

Lateral Displacement Wave

The meridional displacement $r_1(\phi, t)$ of the fluid ring is determined by the combined actions of the η-component of the force exerted on it by the solid boundary and by the inertial forces. Neglecting second-order terms results in the harmonic oscillator equation in the form

$$\frac{\partial^2 r_1}{\partial t^2} = -\frac{f_0}{R_c} r_1 + f_{1\eta} \tag{13}$$

where $\partial r_1/\partial t = w_1(\phi, t)$, as noted before, is the meridional component of the velocity.

Equations (10), (11), and (13) are the principal hydrodynamic results. They are combined subsequently with Euler's rigid-body equation for the vehicle dynamics.

Forces and Moments

The spacecraft is represented as a rigid body, acted upon by the forces and moments that result from the fluid pressure perturbation and by jet damping. The effect of a nutation control system, albeit idealized, also is included.

Fluid Pressure Force and Moment

All perturbation terms of interest to the stability problem are harmonic functions of ϕ, with wavelength $2\pi R_0$. It follows that the incremental fluid pressure force on the vehicle, in the azimuthal interval ϕ to $\phi + d\phi$, has, after transforming to the body-fixed (x, y, z) reference frame, the components

$$dP_{1x} = m_{fl}\, dF_1 \cos\phi, \qquad dP_{1y} = m_{fl}\, dF_1 \sin\phi, \qquad dP_{1z} = 0$$

where

$$dF_1 = \frac{d\phi}{2\pi}\left[\left(\frac{f_0}{h_0} q_1 + f_{1\zeta}\right)\sin\beta_0 + \frac{f_0}{R_c} r_1 \cos\beta_0\right] \tag{14}$$

and where $m_{fl} = 2\pi\rho R_0 b_0 h_0$ is the mass of the fluid. The first term on the right-hand side of Eq. (14) is the result of the surface wave. The second term represents the first-order inertial forces. The third term comes from the lateral displacement of the fluid ring.

The resultant of the fluid pressure forces results in a first-order perturbation $\boldsymbol{a}_1$ of the vehicle center-of-mass acceleration. Designating the ratio of vehicle to fluid mass by $\mu = m_{fl}/m_{vh}$, the components are

$$\begin{aligned} a_{1px} &= \mu \int_{\phi=0}^{2\pi} \cos\phi\, dF_1 \\ a_{1py} &= \mu \int_{\phi=0}^{2\pi} \sin\phi\, dF_1, \qquad a_{1pz} = 0 \end{aligned} \tag{15}$$

The corresponding moment about the vehicle center of mass is designated by $\boldsymbol{M}_{1p}$. The terms that are needed below in expressing Euler's rigid-body equations, to first order, are

$$M_{1px} = -z_0 m_{vh} a_{1py}, \quad M_{1py} = +z_0 m_{vh} a_{1px}, \quad M_{1pz} = 0 \tag{16}$$

Jet Damping

It also is necessary to account for the jet damping force and moment. Jet damping results from the Coriolis force associated with the flow of the combustion gas in the motor chamber and nozzle. The algebraic sign of the force is such that in the absence of slag, damping of the vehicle's precessional motion will occur. A suitable approximation for calculating the force, hence the resulting vehicle acceleration $\boldsymbol{a}_{1j}$, is[18]

$$\begin{aligned} a_{1jx} &= -2(\dot{m}/m_{vh}) z_j \omega_{1y} \\ a_{1jy} &= +2(\dot{m}/m_{vh}) z_j \omega_{1x}, \qquad a_{1jz} = 0 \end{aligned} \tag{17}$$

where $\dot{m}$ is the rocket motor mass flow rate and $z_j(<0)$ is the axial coordinate of the nozzle exit plane (Fig. 2). (In the technical literature, z_j is usually replaced by the difference of the coordinates of nozzle exit plane and propellant burn surface. In practice, however, both formulations give nearly the same result, because the burn surface is usually much closer to the center of mass of the vehicle than is the nozzle exit plane.)

The jet damping moment is given by

$$M_{ijx} = -\dot{m} z_j^2 \omega_{1x}, \qquad M_{1jy} = -\dot{m} z_j^2 \omega_{1y}, \qquad M_{1jz} = 0 \tag{18}$$

Nutation Control

After the nutational instability was discovered in several flights, most spin-stabilized vehicles of the type discussed here were equipped with control thrustors that provide a restoring torque.[19,20] The thrusters have a line of thrust eccentric to the vehicle center of mass and are pulsed periodically whenever the rate gyros indicate an exceedance of the nutation angle beyond a preset threshold. The thrustors are fired during intervals of time that are short compared to the spin period of the vehicle.

In the analysis below, a simpler control law is assumed in which the control thrust, rather than being periodically pulsed, depends sinusoidally on time, with an amplitude that is proportional to the nutation angle excursion (constant gain control). Figure 4 illustrates qualitatively the control torque, designated by M_{1n}. All vectors are projections on the vehicle's transverse plane and rotate clockwise relative to the x, y axes. Figure 4 applies to prolate vehicles for which the rotation is retrograde, i.e., opposite to the spin. Thus, ω_{1t} is the transverse part of the perturbation angular velocity ω_1 and $\boldsymbol{a}_{1p}, \boldsymbol{a}_{1j}, \boldsymbol{a}_{1n}$ are the center-of-mass accelerations resulting from the fluid pressure, jet damping, and nutation control, respectively. Correspondingly, the moments about the center of mass are designated by M_{1p}, M_{1j}, M_{1n}. It is assumed that the control thrustors are located (as usual) forward of the center of mass.

Referring again to Fig. 4, the angle $\psi = \psi(t)$ designates the direction of the transverse angular velocity relative to vehicle fixed axes. The angle ν is the lag angle of the control moment M_{1n} relative to ω_{1t}. In this control law, M_{1n} is taken proportional to ω_{1t}. Thus, defining the (nondimensional) gain N by letting

$$M_{1n} = N m_{vh} \omega_0 z_n^2 \omega_{1t} \tag{19}$$

it follows that the transverse components of the center-of-mass acceleration resulting from the nutation control are

$$\begin{aligned} a_{1nx} &= a_{1n}\sin(\psi + \nu) = N\omega_0 z_n(\omega_{1x}\sin\nu + \omega_{1y}\cos\nu) \\ a_{1ny} &= -a_{1n}\cos(\psi + \nu) \\ &= -N\omega_0 z_n(\omega_{1x}\cos\nu - \omega_{1y}\sin\nu) \\ a_{1nz} &= 0 \end{aligned} \tag{20}$$

The corresponding moments are

$$\begin{aligned} M_{1nx} &= M_{1n}\cos(\psi + \nu) = N m_{vh}\omega_0 z_n^2(\omega_{1x}\cos\nu - \omega_{1y}\sin\nu) \\ M_{1ny} &= M_{1n}\sin(\psi + \nu) \\ &= N m_{vh}\omega_0 z_n^2(\omega_{1x}\sin\nu + \omega_{1y}\cos\nu) \\ M_{1nz} &= 0 \end{aligned} \tag{21}$$

The sums of all perturbation accelerations and moments are

$$\boldsymbol{a}_1 = \boldsymbol{a}_{1p} + \boldsymbol{a}_{1j} + \boldsymbol{a}_{1n}; \qquad \boldsymbol{M}_1 = \boldsymbol{M}_{1p} + \boldsymbol{M}_{1j} + \boldsymbol{M}_{1n} \tag{22}$$

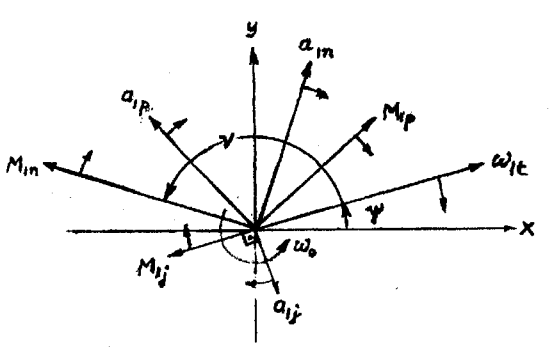

Fig. 4 Diagram of the transverse components of perturbation angular velocity, accelerations, and moments (for prolate vehicle and nutation thrusters forward of center of gravity).

Rigid-Body Equations

Euler's rigid-body equations, when linearized for small nutation angles and applied to inertially symmetric vehicles, are

$$\frac{\partial \omega_{1x}}{\partial t} - (1-\sigma)\omega_0\omega_{1y} = \frac{M_{1x}}{I_t}$$

$$\frac{\partial \omega_{1y}}{\partial t} + (1-\sigma)\omega_0\omega_{1x} = \frac{M_{1y}}{I_t} \tag{23}$$

$$\omega_{1z} = 0$$

Here, the inertia ratio

$$\sigma = I_z/I_t, \qquad (0 < \sigma < 2) \tag{24}$$

is the ratio of the longitudinal moment of inertia I_z to the transverse one I_t of the vehicle.

Normal Mode Analysis

The perturbations from equilibrium are represented by their azimuthal modes. By symmetry, the only ones for which a nontrivial interaction between fluid and vehicle can occur are those with azimuthal wave number $n = \pm 1$.

Disregarding the exceptional case of degenerate eigenvalues, we let

$$v_1/(\omega_0 R_0) = V\exp(s\omega_0 t - i\phi)$$

$$q_1/h_0 = Q\exp(s\omega_0 t - i\phi)$$

$$r_1/R_c = R\exp(s\omega_0 t - i\phi) \tag{25}$$

$$a_{1x}/a_0 = A\exp(s\omega_0 t), \qquad a_{1y}/a_0 = -iA\exp(s\omega_0 t)$$

$$\omega_{1x}/\omega_0 = \Omega\exp(s\omega_0 t), \qquad \omega_{1y}/\omega_0 = -i\Omega\exp(s\omega_0 t)$$

Substitution of Eq. (25) into Eqs. (7) and (13) and collecting all terms proportional to V, Q, R, A, Ω, respectively, results in the following expressions for the components of the sum of the first-order inertial forces:

$$f_{1\phi} = \omega_0^2 R_0[-2R_c'\cos\beta_0\, sR + i\cot\beta_0\, A + iz_p'(1-is)\Omega]\exp(s\omega_0 t - i\phi)$$

$$f_{1\eta} = \omega_0^2 R_0\{(2V + R_c'\cos\beta_0\, R - \cot\beta_0\, A)\cos\beta_0 - [z_0'\cos\beta_0\,(1-is) + \sin\beta_0\,(1+is)]\Omega\}\exp(s\omega_0 t - i\phi) \tag{26}$$

$$f_{1\zeta} = \omega_0^2 R_0\{(2V + R_c'\cos\beta_0\, R - \cot\beta_0\, A)\sin\beta_0 - [z_0'\sin\beta_0(1-is) - \cos\beta_0(1+is)]\Omega\}\exp(s\omega_0 t - i\phi)$$

where

$$R_c' = R_c/R_0, \qquad z_0' = z_0/R_0 \tag{27}$$

Substitution of Eqs. (25) into the integrals in Eq. (15) and making use of the orthogonality of the trigonometric functions results in

$$a_{1px} = \tfrac{1}{2}\mu\Delta\exp(s\omega_0 t)$$

$$a_{1py} = -\tfrac{1}{2}\mu i\Delta\exp(s\omega_0 t), \qquad a_{1pz} = 0 \tag{28}$$

where

$$\Delta = \omega_0^2 R_0\{2\sin^2\beta_0\, V + Q + (R_c'\cos\beta_0\sin^2\beta_0 + \cot\beta_0)R - \cos\beta_0\sin\beta_0\, A - [z_0'\sin^2\beta_0\,(1-is) - \cos\beta_0\sin\beta_0\,(1+is)]\Omega\} \tag{29}$$

There are five equations of motion, viz. Eqs. (10), (11), (13), (22), and (23), that determine the five unknown amplitudes V, Q, R, A, and Ω. The result is obtained by making use of the normal mode expressions (25). First, in Eq. (22) for the three moments, M_{1p} is replaced by $\boldsymbol{a}_{1p}$ by substitution from Eq. (16). In turn, $\boldsymbol{a}_{1p}$ can be expressed by means of Eqs. (28) and (29). Substitution of the expressions (25) for the normal modes then expresses everything in terms of the five complex amplitudes V, Q, R, A, and Ω. M_{1j} and M_{1n}, by means of Eqs. (18) and (21), can be expressed in terms of just Ω as the only unknown amplitude. Second, in Eq. (22) for the three accelerations, $\boldsymbol{a}_{1p}$ is again expressed, as above, by the five amplitudes. The accelerations $\boldsymbol{a}_{1j}$ and $\boldsymbol{a}_{1n}$ by means of Eqs. (17) and (20), respectively, can be expressed in terms of just Ω. Third, in the rigid-body Eq. (23), M_1 is again replaced by the five amplitudes as indicated above. Fourth, substitution of the normal mode expressions into the remaining equations of motion, i.e., Eqs. (10), (11), and (13), expresses them directly in terms of the amplitudes.

When written out in detail as a set of five homogeneous equations for the amplitudes, the equations are too unwieldy to be of much use directly. However, they are useful for taking the limit of small ratios of fluid mass to vehicle mass. This is the case of interest for upper-stage rocket motors because for them this mass ratio is always much smaller than one.

Case of Small Mass Ratios

In spacecraft practice, the case of interest is the one where the mass of the slag is small compared to the mass of the spacecraft. (Slag masses measured in ground tests to date of upper-stage rocket motors usually do not exceed 20 kg.) Retaining in each coefficient of the system of equations only terms up to first order, the result of a fairly lengthy but straightforward calculation can be expressed by the matrix equation

$$S[V, Q, R, A, \Omega]^T = 0 \tag{30}$$

where S is given by

$$S = \begin{bmatrix} -i & s & 0 & 0 & 0 \\ 0 & s^2 - s_Q^2 & j_1 s & j_2 & j_3(1-is) \\ j_4 & 0 & j_5(s^2 - s_R^2) & j_6 & j_7(1-is) + j_8(1+is) \\ \mu j_9 & \mu & \mu j_{10} & j_{11} & j_{12} \\ \mu j_{13} & \mu j_{14} & \mu j_{15} & \mu j_{16} & j_{17} - 2(1-\sigma-is) \end{bmatrix} \tag{31}$$

The coefficients j_1–j_{17} and s_Q^2 and s_R^2 are

$$j_1 = 2iR_c'\cos\beta_0, \qquad j_2 = \cot\beta_0, \qquad j_3 = z_0'$$

$$j_4 = 2\cos\beta_0, \qquad j_5 = -R_c', \qquad j_6 = -\cot\beta_0\cos\beta_0$$

$$j_7 = -z_0'\cos\beta_0, \qquad j_8 = -\sin\beta_0, \qquad j_9 = 2\sin^2\beta_0$$

$$j_{10} = R_c'\cos\beta_0\sin^2\beta_0 + \cot\beta_0, \qquad j_{11} = -2\cot\beta_0 \tag{32}$$

$$j_{12} = 2i\left[2\dot{m}z_j'/(\omega_0 m_{\mathrm{vh}}) - Nz_n' e^{i\nu}\right], \qquad j_{13} = 2R_0'' z_0''\sin^2\beta_0$$

$$j_{14} = R_0'' z_0'', \qquad j_{15} = R_0'' z_0''(R_c'\cos\beta_0\sin^2\beta_0 + \cot\beta_0)$$

$$j_{16} = -R_0'' z_0''\cos\beta_0\sin\beta_0$$

$$j_{17} = 2i\left(\dot{m}z_j''^2/(m_{\mathrm{vh}}\omega_0) - Nz_n''^2 e^{i\nu}\right)$$

$$s_Q^2 = -c_0^2/(\omega_0^2 R_0^2), \qquad s_R^2 = -\left[(R_c'\sin\beta_0)^{-1} - \cos^2\beta_0\right] \tag{33}$$

In addition to R_c' and z_0' already defined in Eq. (27), also introduced here are the nondimensional constants

$$z_j' = z_j/R_0, \qquad z_n' = z_n/R_0, \qquad R_0'' = R_0/R_t$$

$$z_0'' = z_0/R_t, \qquad z_j'' = z_j/R_t, \qquad z_n'' = z_n/R_t \tag{34}$$

where R_t is the transverse gyro radius defined by $I_t = m_{\mathrm{vh}}R_t^2$. The parenthetical expression in Eq. (33) is positive as a consequence of static stability condition (5). Therefore, s_Q and s_R are purely imaginary. For nontrivial solutions of Eq. (30) to exist,

$$\det S = 0 \tag{35}$$

which is the characteristic equation of the eigenvalue problem and requires finding the zeros of the fifth-degree polynomial

$$l_5 s^5 + l_4 s^4 + l_3 s^3 + l_2 s^2 + l_1 s + l_0 = 0 \qquad (36)$$

For brevity, the coefficients l_0–l_5 are not tabulated here. (A complete listing suitable for programming can be obtained by writing to the author.) They can, however, be found efficiently by any software that allows algebraic symbolic operations. The procedure consists therefore in evaluating det S and collecting terms with equal powers of s. Finding then the roots of Eq. (36) is best done by using one of the numerous available software programs, such as the robust programs based on the Jenkins–Traub method (e.g., in the International Mathematical Society Library). The system is stable if there are no roots with a nonnegative real part.

A partial check on the programming can be obtained by setting the fluid mass equal to zero. In this case, it follows from the fifth row of S that

$$j_{17} - 2(1 - \sigma - is) = 0$$

which, when solved for s and substitution is made for j_{17}, gives

$$s = -i(1 - \sigma) - \dot{m} z_j'^2 / (m_{vh}\omega_0) + N z_n'^2 (\cos\nu + i \sin\nu)$$

In the absence of both jet damping and nutation control, all vectors, such as a_1 and ω_1, vary sinusoidally with an angular frequency $(1 - \sigma)\omega_0$, as expected. The results of a sample calculation are given in the Results section.

Results

To illustrate the theoretical development, a vehicle is assumed for reference purposes with the following parameters: An inertially symmetric, prolate vehicle with inertia ratio $\sigma = 0.50$, mass $m_{vh} = 1000$ kg, thrust $T_0 = 50{,}000$ N, nominal rate of spin $\omega_0 = 10.0$ rad/s, mass flow rate $\dot{m} = 25$ kg/s, $R_0 = 0.25$ m, $z_0 = -2.00$ m, $R_c = 0.50$ m, $R_t = 0.71$ m, $z_j = -2.50$ m, $z_n = +2.50$ m.

The loci of the roots in the complex plane of s, as functions of the fluid mass m_{fl}, are shown in Fig. 5 for four cases (with and without jet damping, and with and without nutation control). In all cases, as is evident, only one of the five branches can lead to the coning instability, and this only above and below certain amounts of fluid mass. For the conditions applying to Fig. 5a, these limits are between 9 and 46 kg. A comparison of Figs. 5a and 5b shows that the effect of jet damping is relatively small and that it does not remove the instability. This is in accord with experience gained from flight tests.

The unstable roots indicate for the reference vehicle a maximum growth rate of the instability at about 20–30 kg of slag. This number is consistent with, although somewhat higher than, what is observed in typical ground tests.[13]

At the peak growth rate, when (as is the case in the flight tests discussed earlier) there is jet damping but no control, $m_{fl} = 26$ kg and the real part of s is $s_r = 0.037$. This result of the theory therefore corresponds to an exponential growth rate of $\omega_0 s_r = 0.37$ s^{-1}. On the other hand, the growth rate observed in flight tests was 0.42 s^{-1} (the mean of 12 flights). Considering that all flight vehicles had

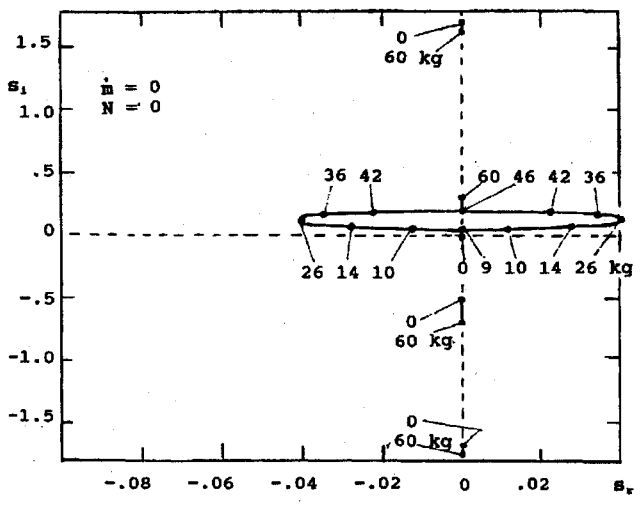

a) Without jet damping or control

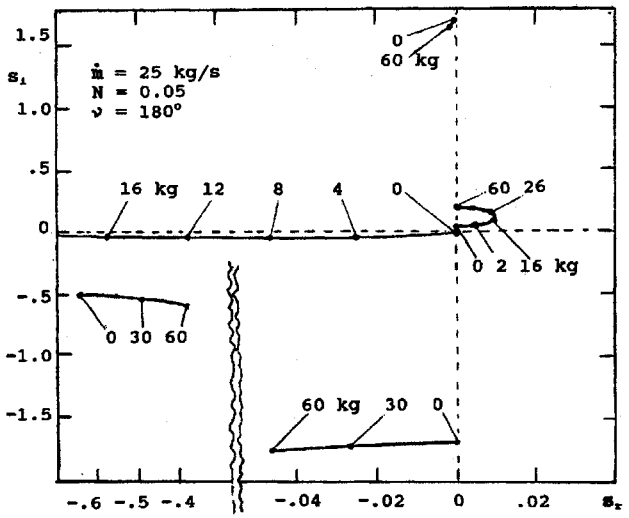

c) With jet damping and control gain $N = 0.05$, $\nu = 180$ deg

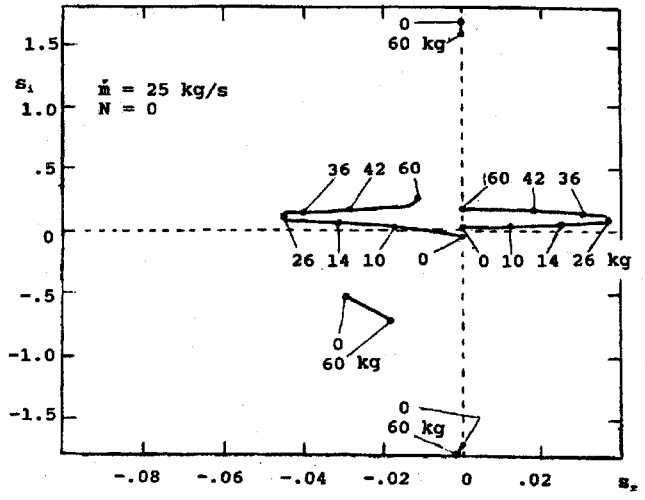

b) With jet damping, no control

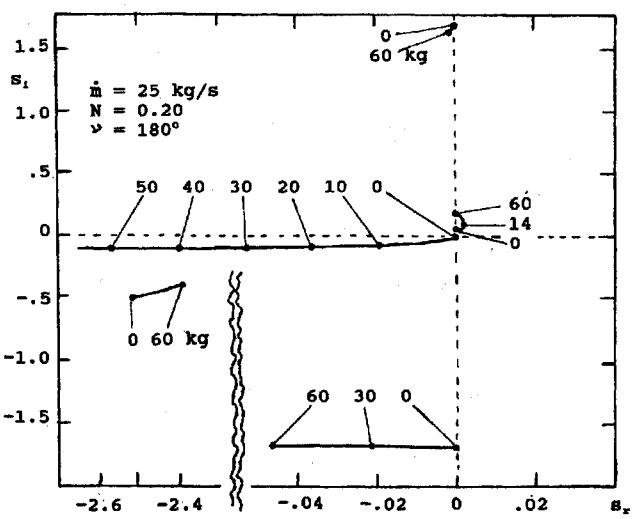

d) With jet damping and control gain $N = 0.20$, $\nu = 180$ deg.

Fig. 5 Loci of the five roots of the polynomial Eq. (36) as functions of the fluid mass.

somewhat different masses and inertial properties (although all used the same motor), this result clearly supports the theoretical results.

Adding a nutation control based on the control law (19), with a lag angle ν of 180 deg and a gain $N = 0.20$, the maximum real part of s is 0.0030, which corresponds to an exponential growth rate of the instability of 0.030 s^{-1}, hence a factor of about 10 less than without the control. For the type of solid-propellant motors considered here, the time interval during which the instability manifests itself is roughly 30 s. This growth rate of 0.030 s^{-1}, although still positive, in practice is inconsequential. The calculation points out, however, that the simple, open-loop control law (19) is far from optimum.

The instability growth rate, as calculated here, is based on a constant vehicle and slag mass as they may be instantaneously present. This is allowed because the mass changes are slow compared to the vehicle's precession rate. For a more accurate computation, the actual masses at each instant would have to be calculated, followed by an integration over time of the nutation angle.

Conclusions

The paper confirms the explanation, first advanced by others, that the coning instability observed with certain upper-stage vehicles is caused by the liquid slag retained in the motor. By comparison, the gasdynamic effect, although also destabilizing, is of minor importance.

Earlier work is extended by including a hydrodynamic description of the motion of the slag in the motor recess that supports both free-surface waves and sloshing along the solid boundaries. The model allows one to correlate the growth rate of the instability with the slag mass present. The results are consistent with the instability growth rates observed in actual flights, and also, at least qualitatively, with slag masses measured in ground tests of the motors.

The theory also confirms what had already been known from the analysis of flight tests, that jet damping has only a relatively minor beneficial effect. A simple control law, designed to suppress the instability, has been considered and is included in the analysis.

Appendix: Circular Boundary

If the boundary containing the fluid has an approximately constant curvature in the meridional plane, the mean fluid height h_0 can be estimated without a case-by-case integration. The approximation is based on representing the boundary and the free surface by second-degree polynomials in z. The strong inequalities $h_0 \ll b_0 \ll R_0$ are assumed, where b_0 is the distance between the two shore lines for the reference condition.

With R designating the cylindrical radius of a point on the free surface, β the angle of the normal to this surface with the z axis, it follows that $\tan\beta = \omega_0^2 R/a_0$. Differentiating, replacing β by its mean value β_0, and making use of Eq. (4),

$$\frac{R_f}{R_0} = \frac{1}{\cos^2\beta_0 \sin\beta_0} \tag{A1}$$

where R_f is the mean radius of curvature of the reference free surface.

Integrating for the area A_0 enclosed between the boundary and the reference free surface, one finds

$$b_0 = \left(\frac{12A_0}{1/R_c - 1/R_f}\right)^{\frac{1}{3}} \tag{A2}$$

where R_c is the local radius of curvature of the boundary. With the same approximation

$$A_0 = \frac{m_{fl}}{2\pi R_0 \rho} \tag{A3}$$

The mean fluid height then follows easily from Eqs. (A1–A3) and (9).

Acknowledgment

This work was supported in part by NASA Grant NAGW-4254. The author thanks the following for numerous discussions of the coning instability: M. Caldwell and E. Webster of McDonnell Douglas Aircraft Corp., J. E. McIntyre, Hughes Aircraft Co., and E. Landsbaum of The Aerospace Corp. The author also wishes to thank K. Lee for programming and obtaining all numerical results.

References

[1]Meyer, R. X., "Coning Instability," TM 82-1175, The Aerospace Corp., El Segundo, CA, Jan. 1982.

[2]Meyer, R. X., "Convective Instability in Solid Propellant Rocket Motors," *Advances in Astronautical Sciences*, Vol. 54, Oct. 1983, p. 173 (AAS Paper 83-368).

[3]Flandro, G. A., "Interaction of Inertial Waves in a Spinning Solid Propellant Rocket Motor with Spacecraft Motion," U.S. Air Force Rocket Propulsion Lab. Rept., Edwards AFB, CA, Oct. 1982.

[4]Flandro, G. A., "Fluid Mechanics of Spinning Rockets," U.S. Air Force Rocket Propulsion Lab. Rept. TR-86-072, Edwards AFB, CA, Jan. 1987.

[5]Walters, A. G., "Non-Symmetric Flow in Laval Type Nozzles," *Philosophical Transactions of the Royal Society of London Series A: Mathematical and Physical Sciences*, Vol. 273, A 1232, 1972, pp. 185–235.

[6]Pirumov, U. G., and Roslyakov, G. S., *Gas Flow in Nozzles*, Vol. 29, Springer Series in Chemical Physics, Springer–Verlag, Berlin, 1986 (English translation).

[7]Varwig, R. L., Whittier, J. S., Duran, D. A., and Meyer, R. X., "Aerodynamic Side Force Induced by Nozzle Entrance Flow Asymmetry," *Journal of Spacecraft and Rockets*, Vol. 26, No. 4, 1989, pp. 217–220.

[8]Misterek, D. L., Murdock, J. W., and Koshigoe, S., "Gas Dynamic Flow in a Spinning, Coning Solid Propellant Motor," *Journal of Propulsion and Power*, Vol. 9, No. 1, 1993, pp. 35–41.

[9]McIntyre, J. E., and Tanner, T. M., "Fuel Slosh in a Spinning On-Axis Propellant Tank: An Eigenmode Approach," *Space Communication and Broadcasting*, Vol. 5, No. 4, 1987, pp. 229–251.

[10]Staunton, B. D., and Smit, G. N., "The Analysis and Simulation of PAM-S Coning Instability, Vol. 3: Slag Dynamics," The Aerospace Corp., TR TOR-0091-6464-06-1, El Segundo, CA, 1991.

[11]Tingle, S. D., and Landsbaum, E. M., "Slag Estimation for Solid Rocket Motors," 1983 JANNAF Propulsion Meeting, Paper 12, Oct. 1990.

[12]Haloulakos, V. E., "Rocket Motor Slag Formation: Effects of Internal Flow Field and Propellant Grain Configuration," *Proceedings of the 1985 JANNAF Propulsion Meeting*, San Diego, CA, Vol. 1, Publ. 425, 1985, p. 89.

[13]Meyer, R. X., "In-Flight Formation of Slag in Spinning Solid Propellant Motors," *Journal of Propulsion and Power*, Vol. 8, No. 1, 1992, pp. 45–50.

[14]Mingori, D. L., and Yam, Y., "Nutational Instability of a Spinning Spacecraft with Internal Mass Motion and Axial Thrust," *AIAA/AAS Astrodynamics Conference Proceedings* (Williamsburg, VA), AIAA, New York, 1986, pp. 367–375 (AIAA Paper A86-47901).

[15]Mingori, D. L., Halsmer, D. M., and Yam, Y., "Stability of Spinning Rockets with Internal Mass Motion," American Astronomical Society, AAS Paper 93-135, Pasadena, CA, Feb. 1993.

[16]Lamb H., *Hydrodynamics*, 6th ed., Dover, New York, 1932, Chap. 8.

[17]Bloor, M. I. G., "Effect of Viscosity on Long Waves in Shallow Water," *Physics of Fluids*, Vol. 13, No. 6, 1970, pp. 1435–1439.

[18]Thomson, W. T., and Reiter, G. S., "Jet Damping of a Solid Rocket: Theory and Flight Results," *AIAA Journal*, Vol. 3, No. 3, 1965, pp. 413–416.

[19]Brennan, P., "PAM-S Nutation Control System Capability Study," McDonnell Douglas Aircraft Corp., Memorandum A3-P930-DLT-89-159, Sept. 1989.

[20]Stevaston, G. E., "PAM-S Booster Control System Analysis," Jet Propulsion Lab. Rept. D-6289, California Inst. of Technology, Pasadena, CA, Oct. 1989.

F. H. Lutze Jr.
Associate Editor